Inorganic Chemistry

pubs.acs.org/IC Article

Toward Near-Infrared Emission in Pt(II)-Cyclometallated Compounds: From Excimers' Formation to Aggregation-Induced Emission

Ariadna Lázaro, Ramon Bosque, Jas S. Ward, Kari Rissanen, Margarita Crespo, and Laura Rodríguez*

Cite This: https://doi.org/10.1021/acs.inorgchem.2c03490 Read Online

ACCESS | Metrics & More | Article Recommendations | Supporting Information

ABSTRACT: Two series of Pt(II)-cyclometallated compounds containing N^C^N tridentate and alkynyl-chromophore ligands have been synthesized and structurally characterized. The N^C^N ligands differ on the presence of R_1 = H or F in the central aromatic ring, while six different chromophores have been introduced to the alkynyl moiety. Single-crystal X-ray structures for some of the compounds reveal the presence of weak intermolecular contacts responsible for the formation of some dimers or aggregates. The photophysical characterization shows the presence of two emission bands in solution assigned to the $^3\pi-\pi^*$ transition from the N^C^N ligands mixed with ^{3}MLCT/^{3}ILCT transitions (higher energy band) in deaerated samples. The formation of excimers has also been identified as a broad band at longer wavelengths [near-infrared (NIR) emission] that becomes the main emission band for compounds containing phenanthrene as the chromophore. NIR emission behavior has also been explored using acetonitrile/water mixtures, and the presence of aggregates that emit at ca. 650 nm has also been detected.

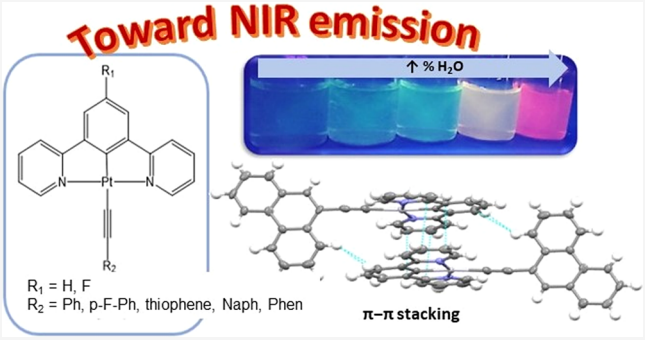

■ INTRODUCTION

Luminescent transition metal complexes display several applications in a variety of fields such as device fabrication, molecular probes, sensors, or organic light-emitting diodes (OLEDs) among others, and the research in this field has rapidly increased in the last few years due to their intrinsic photophysical properties.[1−3] They have been observed to display in some cases better properties in comparison to organic fluorophores, such as enhanced photostability (that allows continuous exposure of the complexes to irradiation), long luminescence lifetimes (from hundreds of nanoseconds to microseconds or even milliseconds) that allow the elimination of interference from the autofluorescence background, and the possibility to tune room temperature phosphorescence.

The d^8 platinum(II) complexes are particularly relevant since they present unique supramolecular self-assembly properties that are not observable in the octahedral d^6 and tetrahedral d^{10} metal complexes. They present square-planar geometries that can undergo face-to-face intermolecular interactions through ligand−ligand and Pt(II)···Pt(II) interactions, which can give rise to new electronic excited states that produce red-shifted emission from triplet metal−metal-to-ligand charge-transfer (^{3}MMLCT) or excimeric ^{3}IL excited states in addition to the one arising from the mononuclear Pt(II) moiety.[1,4−12] These assemblies are of great relevance to modulate the resulting photophysical properties, both regarding their energy and emission intensity by subtle changes to their environment. It should be taken into consideration that aggregation can happen in the ground state (dimers) or the excited state (excimers). Additionally, Pt(II), as a heavy atom, induces strong spin−orbit coupling, favoring the population of the T1 triplet excited state by enhanced intersystem crossing from S1 → T1 and producing phosphorescence at room temperature.[4,13]

The use of cyclometallating ligands is a convenient strategy to favor luminescence since the strong field of these ligands tends to favor emission efficiencies as they raise the energies of deactivating metal-centered states, reducing non-radiative deactivation pathways. Tridentate cyclometallated ligands are particularly relevant since they have been observed to induce higher rigidity on the complex with respect to bidentate ligands, inhibiting distortion and reducing non-radiative deactivation processes.[3]

Received: October 4, 2022

Scheme 1. Synthesis of Cyclometallated Platinum(II) Compounds[a]

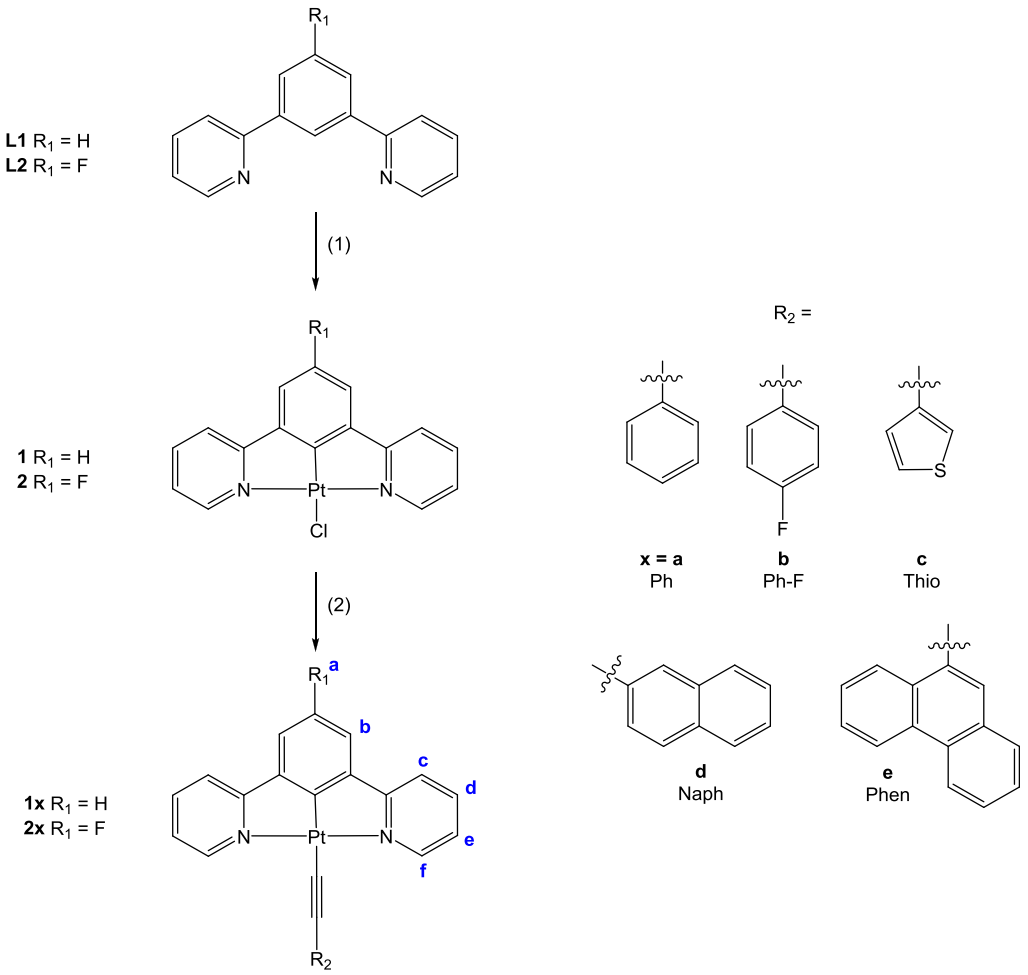

[a](1) K_2PtCl_4, acetic acid/water 9:1, microwave heating, 160 °C, 30 min. (2) R_2-C≡C-H, NaOH, methanol, r.t., 24 h. The labeling convention used for NMR results is shown for the new compounds.

The nature of the cyclometallated ligands and co-ligands and the ionic or neutral character of the molecules are extremely relevant to modulate the absorption and emission properties. Thus, the study of Pt(II)-cyclometallated compounds is currently a highly relevant research field in order to achieve high luminescence (mainly from the triplet excited state, i.e., phosphorescence) quantum yields, color tunability, and stability.[7,14,15] In particular, C^N^N and N^C^N coordination modes are more commonly found in tridentate cyclometallating ligands, and they have been observed to exhibit intense luminescence and versatile emissive excited states, including not only intraligand (IL) (π−π^*) excited states but also the excimeric excited states.[16−18] Among them, N^C^N coordination seems to favor higher emission intensities and quantum yields.[9] Fewer efforts have been made on the analysis of the co-ligand that occupies the fourth coordination position at the Pt(II) center, even though they can also have an influence on their resulting assemblies and luminescent properties.[19]

An interesting tangent in the field is the modulation of the chemical structures and assemblies to shift the emission to the red since, for example, OLEDs and materials that emit in the infrared (IR) or near-infrared (NIR) region represent a challenging target due to the favored deactivation processes in low-energy emissive populated states.[20] IR and NIR emission is of vital importance in several relevant applications such as full-color displays, remote sensing of environmental conditions, night-vision displays, bio-chemosensors, in vivo imaging, light-fidelity (Li-Fi) communication, or security authentication devices, and it is mostly explored with pure organic molecules.[21−25] Different strategies can be followed to modulate the final emission of the complexes to red, with excimers' formation and aggregation-induced emission (AIE) being popular design methodologies.[10,20,22,26−30]

In this work, we have designed and synthesized two series of Pt(II)-cyclometallated complexes containing tridentate N^C^N ligands with an alkynyl chromophore as the co-ligand occupying the fourth coordination position. The different chromophores have been chosen in order to evaluate how the electron-withdrawing character (fluorine), soft atom (sulfur in thiophene), or extended aromaticity (benzene, naphthalene, and phenanthrene) can affect the resulting packing through intermolecular contacts affecting their luminescence. Additionally, the two series of compounds differ on the presence of a H or F atom at the central benzyl ring, which could also confer different intermolecular forces in the packing. The differences in the resulting photophysical properties depending on the N^C^N ligand and co-ligands have been analyzed in detail together with the resulting AIE processes, with those being observed to shift the emissions up to ca. 700 nm, thanks to excimer and aggregate formation.

https://doi.org/10.1021/acs.inorgchem.2c03490
Inorg. Chem. XXXX, XXX, XXX−XXX

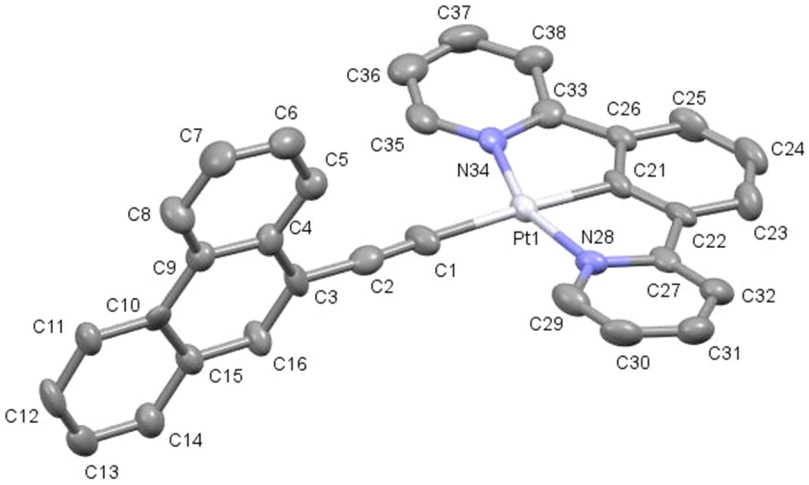

Figure 1. Molecular structure of compound **1e**. Selected bond lengths (Å) and angles (°) with estimated standard deviations: Pt(1)−N(34): 2.038(7); Pt(1)−C(21): 1.939(7); Pt(1)−N(28): 2.035(7); Pt(1)−C(1): 2.077(8); C(1)−C(2): 1.181(11); N(34)−Pt(1)−C(21): 79.4(3); C(21)−Pt(1)−N(28): 79.7(3); N(28)−Pt(1)−C(1): 100.2(3); C(1)−Pt(1)−N(34): 100.9(3); Pt(1)−C(1)−C(2): 177.71(9). The thermal ellipsoids are drawn at the 50% probability level, and hydrogen atoms are omitted for clarity.

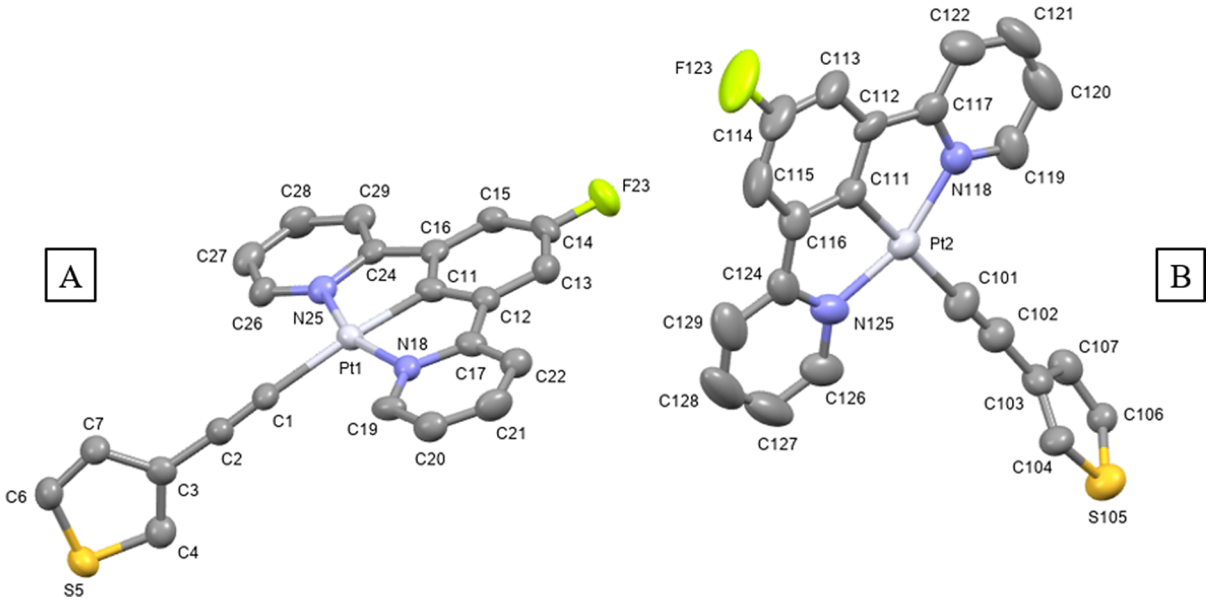

Figure 2. Molecular structure of compound **2c** (two crystallographically independent molecules present in the asymmetric unit cell, A and B). Selected bond lengths (Å) and angles (°) with estimated standard deviations: (A) Pt(1)−N(18): 2.033(5); Pt(1)−C(11): 1.942(7); Pt(1)−N(25): 2.035(5); Pt(1)−C(1): 2.099(7); C(1)−C(2): 1.179(9); N(18)−Pt(1)−C(11): 80.0(3); C(11)−Pt(1)−N(25): 80.1(3); N(25)−Pt(1)−C(1): 98.0(2); C(1)−Pt(1)−N(18): 101.7(2); Pt(1)−C(1)−C(2): 165.2(6). (B) Pt(2)−N(118): 2.040(5); Pt(2)−C(111): 1.930(8); Pt(2)−N(125): 2.038(7); Pt(2)−C(101): 2.054(8); C(101)−C(102): 1.185(10); N(118)−Pt(2)−C(111): 80.1(3); C(11)−Pt(2)−N(125): 79.3(3); N(125)−Pt(2)−C(101): 99.9(3); C(101)−Pt(2)−N(118): 100.8(3); Pt(2)−C(101)−C(102): 178.7(6). The thermal ellipsoids are drawn at the 50% probability level, and hydrogen atoms are omitted for clarity.

■ RESULTS AND DISCUSSION

Synthesis and Characterization. All compounds were synthesized by following the route summarized in Scheme 1. As reported in the literature, the corresponding precursors **1** and **2** were reacted with different alkynyl aromatic ligands with sodium hydroxide as a base.[31] Final compounds **1x** and **2x** were obtained as orange solids with moderate yields (54−80%) after precipitation and washing with water, methanol, and hexane.

Characterization of the synthesized compounds by ^{1}H NMR spectroscopy showed the disappearance of the terminal alkynyl proton (R_2-C≡C-***H***) from the corresponding alkynyl aromatic ligand. This observation together with the appearance of the aromatic protons of the new ancillary ligand confirms the correct substitution of the chlorido and formation of the desired platinum complexes. A significant downfield shift in the pyridine proton (H^f) of ca. 0.10−0.25 ppm is observed when compared with the precursors (9.36−9.38 ppm). However, its coupling constant with the platinum atom is not affected since the ligand *trans* to the nitrogen of the pyridine bond is not exchanged (Figures S1−S9). For family **2x**, all compounds were also characterized by ^{19}F NMR spectroscopy, observing only one signal as a triplet due to the coupling with the two adjacent aromatic protons of the central ring. A second signal

https://doi.org/10.1021/acs.inorgchem.2c03490
Inorg. Chem. XXXX, XXX, XXX−XXX

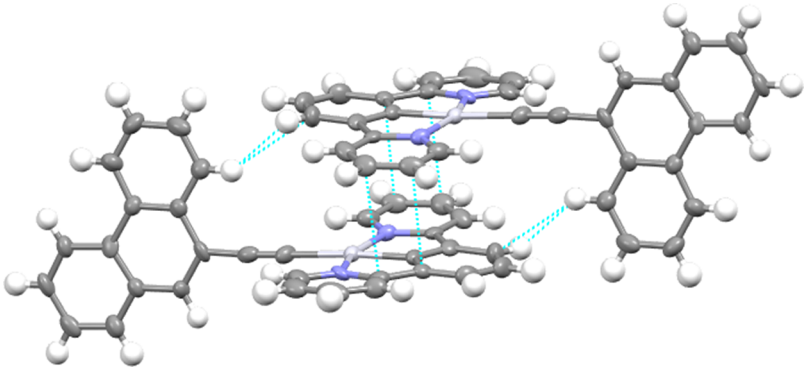

Figure 3. View of the relevant intermolecular short contacts for compound **1e** highlighted in blue: $\pi\cdots\pi$: 3.361 and 3.345 Å; C···H: 2.849 Å. Gray, platinum; blue, nitrogen.

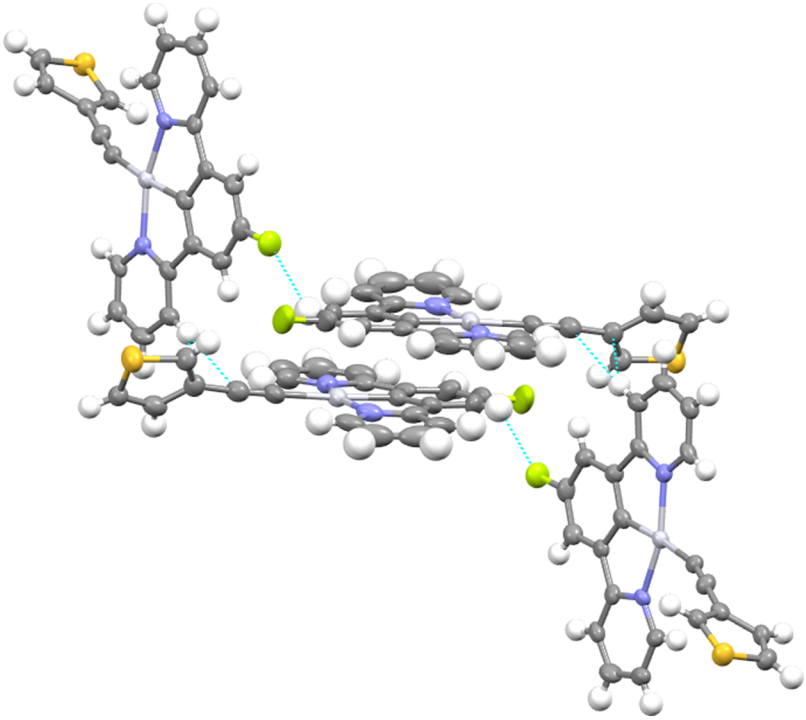

Figure 4. View of the relevant intermolecular short contacts for compound **2c** highlighted in blue: F···H: 2.449 Å; C···H: 2.870 Å. Gray, platinum; blue, nitrogen; yellow-green, fluorine; orange, sulfur.

is present in the NMR spectrum of compound **2b** due to the aromatic *p*-fluorobenzene moiety (Figures S10−S15).

The C≡C (around 2070 cm^{-1}) vibration as well as the disappearance of the band assigned to the stretching of the terminal proton of the free alkynyl moiety (around 3300 cm^{-1}) was determined by IR spectroscopy. Further confirmation of the successful formation of the products was checked by electrospray ionization [ESI(+)] mass spectrometry finding the protonated molecular peak for all cases (Figures S16−S24).

Single crystals suitable for X-ray diffraction analysis were grown for compounds **1e** and **2c** (s71) by slow diffusion of methanol or hexane, respectively, into a concentrated dichloromethane solution of the compound. Compound **1e** presents one single molecule in the asymmetric unit, while for compound **2c**, two crystallographically independent molecules are observed (Figures 1 and 2). As shown in Figures S25 and S26, the unit cell of both compounds contains four molecules. The platinum atom adopts the expected square-planar environment completed by the tridentate [N^C^N] ligand and the alkynyl group. Bond distances and angles are in agreement with those reported in the literature for analogous [N^C^N] platinum(II)-cyclometallated compounds.[32,33] The aromatic ring attached to the alkynyl moiety is almost perpendicular to the cyclometallated unit for compound **1e** (85.3°), while for the two molecules in the asymmetric unit of compound **2c**, they are observed in two different conformations with angles of 52.1° and 83.3°.

The packing for both compounds presents a zig-zag conformation held together by the stacking of two cyclometallated moieties (Figures S25 and S26). These dimeric structures are arranged in a head-to-tail fashion, which does not permit the presence of metallophilic interactions in **1e** (with a Pt···Pt distance of 5.0521(5) Å). A similar distance was observed for Pt2···Pt2 of 4.9888(4) Å in **2c**. However, in **2c**, a much shorter Pt···Pt distance of 3.4654(4) Å was observed for Pt1···Pt1, which is just below the combined van der Waals radius (3.5 Å) for this interaction.[31] As depicted in Figure 3, for compound **1e**, these dimer-like structures are due to the

https://doi.org/10.1021/acs.inorgchem.2c03490
Inorg. Chem. XXXX, XXX, XXX−XXX

Table 1. Electronic Absorption and Emission Data Including Absorption and Phosphorescence Emission Maxima and Phosphorescence Quantum Yields Recorded in Air-Equilibrated (with O_2) or Degassed (N_2 sat.) Dichloromethane Solutions at Room Temperature

compound	λ_{abs}, nm ($\varepsilon \times 10^{-3}$, M^{-1} cm^{-1})	λ_{em} (nm)	ϕ_{Ph} (with O_2)	ϕ^0_{Ph} (N_2 sat.)	ϕ^0_{Ph} monomer (N_2 sat.)	ϕ^0_{Ph} excimer (N_2 sat.)
L1	280 (8.6)	341	0.004	0.004	0.004	
L2	279 (8.9)	337	0.007	0.007	0.007	
1	290 (18.4), 333 (5.8), 380 (7.2), 402 (5.9)	490	0.034	0.605	0.605	
2	290 (12.5), 378 (4.2), 422 (4.7)	505	0.030	0.660	0.660	
1a	291 (17.0), 389 (4.6)	497, 702	0.039	0.605	0.456	0.149
1b	290 (18.2), 388 (5.5)	495, 692	0.045	0.558	0.390	0.168
1c	292 (25.5), 391 (7.0)	501, 698	0.032	0.518	0.357	0.161
1d	288 (8.7), 309 (5.8), 389 (2.3)	490, 693	0.041	0.547	0.447	0.100
1e	289 (28.4), 319 (22.3), 334 (24.0), 391 (7.7)	547, 698	0.012	0.342	0.130	0.212
2a	289 (10.1), 380 (3.5), 421 (3.5)	507, 692	0.040	0.596	0.485	0.111
2b	292 (20.6), 390 (5.5), 422 (5.7)	511, 694	0.028	0.491	0.340	0.151
2c	291 (10.8), 391 (2.7), 424 (2.8)	513, 696	0.033	0.587	0.455	0.132
2d	294 (31.5), 310 (2.5), 392 (6.8), 427 (7.5)	520, 699	0.027	0.506	0.274	0.232
2e	290 (32.1), 319 (25.6), 333 (26.6), 425 (8.2)	547, 700	0.011	0.373	0.069	0.304

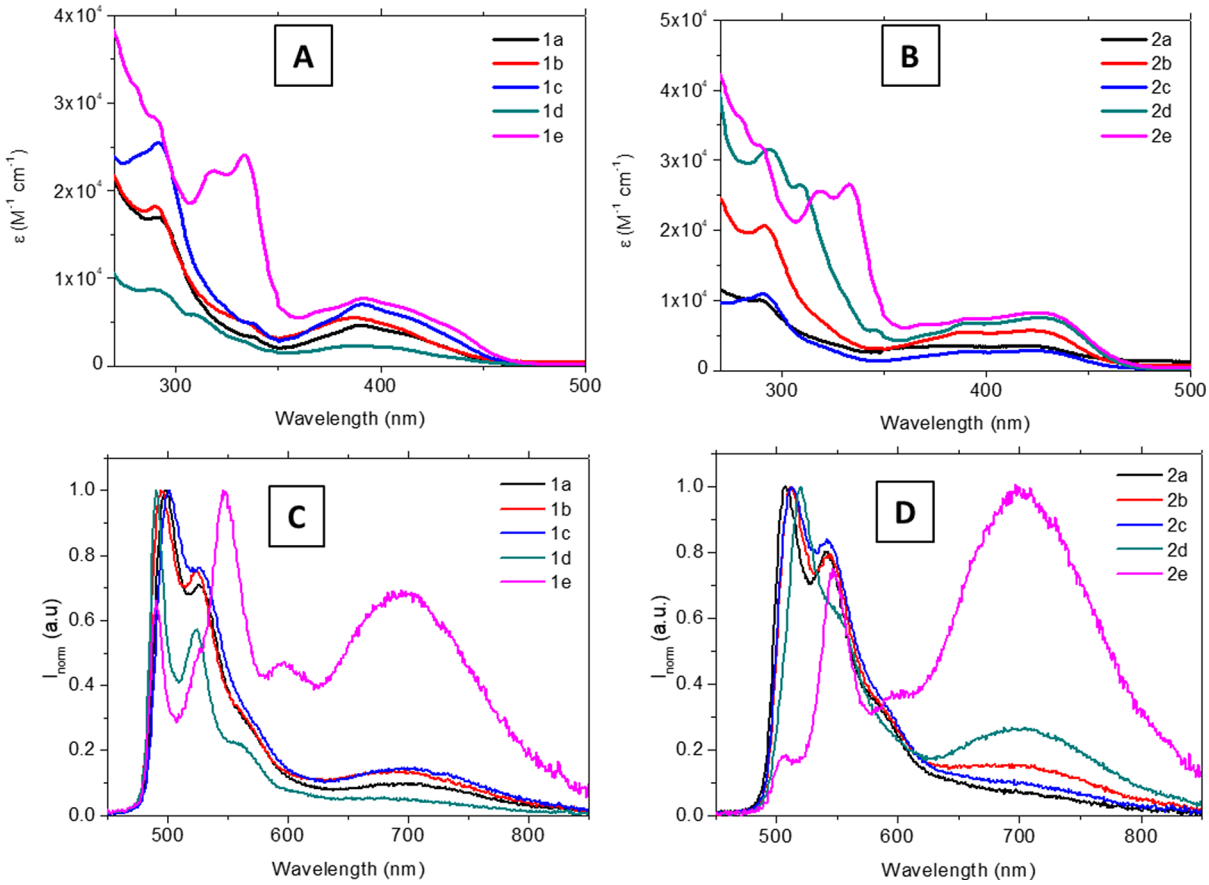

Figure 5. Absorption spectra (A for series **1** and B for series **2**) and normalized emission spectra (C for series **1** and D for series **2**) for N_2-saturated 5×10^{-5} M dichloromethane solutions of the compounds at 298 K (λ_{exc} = 390 nm).

presence of $\pi-\pi$ stacking (3.36 and 3.35 Å) and C···H (2.85 Å) intermolecular short contacts, which results in an interplanar distance of 3.0 Å. Additional C−H···π intermolecular contacts of 3.03 Å between the phenanthrene groups of two adjacent molecules can be identified, which could be responsible for different emissive properties (see below). However, for compound **2c**, we can only observe F···H: 2.45 Å and C···H: 2.87 Å interactions, leading to a higher interplanar distance of 3.2 Å (Figure 4).

Photophysical Characterization. The absorption spectra of all compounds (final products **1a−e** and **2a−e** and precursors) were recorded in 5×10^{-5} M dichloromethane solutions at 298 K, and the results are shown in Figures S27−S29 and Table 1. In the higher energy region (270−350 nm), all compounds present intense bands that can be attributed to $^1\pi-\pi^*$ IL transitions of the cyclometallated 1,3-di(2-pyridyl)-benzene, which are also recorded in the absorption of the free ligands **L1** and **L2** (Figure S30), overlapped, in some cases, with $^1\pi-\pi^*$ IL transitions of the alkynyl aromatic moiety. In

https://doi.org/10.1021/acs.inorgchem.2c03490
Inorg. Chem. XXXX, XXX, XXX−XXX

the lower energy region (350−450 nm), less intense bands are observed, which can correspond to mixed charge-transfer and ligand-centered character transitions, according to the literature.[7−9,12,16,26,28,34−36]

The samples were excited at their lower energy absorption band, and the recorded emission spectra display a vibronically structured band centered around 500 nm (Figure 5) that can be attributed to a primarily ligand centered $^3\pi-\pi^*$ transition from the N^C^N ligands that can be mixed with ^{3}MLCT/^{3}ILCT transitions, involving the cyclometallated ligand. The same pattern has been recorded in the emission of the chlorido precursors (Figure S31).[3,4,8,12,16,36] The large Stokes shift and the quenching of the emission in the presence of oxygen support their phosphorescent emission assignment (Table 1). The free **L1** and **L2** ligands present a broad emission band around 350 nm, which can be assigned to a fluorescent $^1\pi-\pi^*$ IL transition that is not quenched by the presence of oxygen (Figure S32), proving that the phosphorescent emission of these compounds is due to the perturbation from the platinum atom. Another band centered at 700 nm is observed for all final platinum complexes **1a−e** and **2a−e**, which can be assigned to excimer formation.[7,37] The excimer assignment can be done, thanks to the excitation spectra that resemble the same pattern (that fits the absorption spectra) when the emission is collected at the two maxima (500 and 700 nm, see Figure S33). The lack of excimer formation recorded for **1** and **2** together with the different excimer intensities recorded in the different cases indicates the main role of the alkynyl-R_2 chromophore in the excimer formation. This excimer is observed to be more favored for series **2** complexes and mainly for the more extended chromophore, phenanthrene, in compound **2e**. In fact, excimer emission has been previously reported in the literature for other LPt-Cl analogues to **1** and **2** only at higher concentrations.[38] The total phosphorescence quantum yields (QY) increase in deaerated solutions, reaching values up to 60%, similar to the values reported for analogous compounds.[28,39] Global QY values have been split into their monomer and excimer contribution (Table 1), and it can be observed that, in general, the monomer emission is the major radiative deactivation pathway. Instead, the excimer has a larger contribution only for the phenanthrene derivatives **1e** and **2e**, with almost a total dominance in compound **2e** (Table 1 and Figure 5). This could be ascribed to the establishment of $\pi-\pi$ intermolecular contacts in solution between the phenanthrene groups that have been identified to be very close to each other in the three-dimensional X-ray crystal packing in the solid state of **1e** (Figure S25). Thus, although no significant differences have been observed in the global QY values of the platinum complexes when the two series of compounds are compared, some significant differences can be observed when the emission efficiency is split between the two contributions (monomer and excimer). In this case, the principal parameters that seem to have the main effect are the extended aromaticity (a larger contribution of the excimer for **1e** and **2e**) and the H or F atom at the central N^C^N tridentate ligand, with a larger effect in the presence of a fluorine in the excimer formation. This may be due to the resulting less electronic density in the phenanthrene aromatic ring, making them more suitable for establishing intermolecular contacts.

Phosphorescence emission lifetimes were recorded for both the monomer and the excimer emission transitions and are of hundreds of nanoseconds. These values increase to a few microseconds in deaerated solutions, and they are in the range of those reported previously in the literature for similar compounds (Table 2) and support triplet emission origin.[4,28,40,41] The recorded values for the final platinum complexes are, in general, in the same order as those recorded for the platinum precursors **1** and **2**. Phenanthrene derivatives **1e** and **2e** are again a particular case that displays longer decay time values than the rest of the compounds as previously observed for other platinum cyclometallated compounds containing this chromophore.[4] Time-resolved phosphorescence spectra were studied for these two compounds (**1e** and **2e**), and the resulting kinetics show the clear predominance of the monomer emission with respect to the excimer at increasing time-gating in agreement with the longer decay times recorded (see Figure S34).

Table 2. Phosphorescence Lifetimes of the Compounds Recorded in Air-Equilibrated (with O_2) or Degassed (N_2 sat.) Dichloromethane Solutions

compound	τ (μs) monomer (with O_2)	τ (μs) excimer (with O_2)	τ° (μs) monomer (N_2 sat.)	τ° (μs) excimer (N_2 sat.)
L1	3.91×10^{-3}			
L2	2.26×10^{-3}			
1	0.42		8.33	
2	0.39		6.90	
1a	0.32	0.16	5.25	2.94
1b	0.44	0.20	7.35	3.28
1c	0.22	0.11	4.55	2.99
1d	0.22	0.14	4.91	2.94
1e	0.38	0.29	41.39	5.27
2a	0.54	0.22	5.87	3.12
2b	0.42	0.19	6.96	3.00
2c	0.37	0.16	5.37	2.66
2d	0.45	0.16	7.24	3.68
2e	0.560	0.34	34.44	6.88

Radiative and non-radiative rate constants have been calculated in all cases from the experimental quantum yields and lifetime values (Table S2). According to these values, the increase in the recorded quantum yields from the monomer emission band in deaerated samples can be ascribed mainly to a significant decrease of the non-radiative deactivation pathway rate. We can observe that k_{nr} values are one order of magnitude smaller than those in air-equilibrated samples, while k_r values stay similar. Additionally, looking at the excimer emission band, we can observe that the k_{nr} values for phenanthrene derivatives **1e** and **2e** are smaller than those calculated for the other platinum complexes, in agreement with the significant increase in the emission intensity of this band.

In the solid state (powder), all compounds present a broad emission band centered between 579 and 626 nm (Figure S35 and S36). This emission band can be assigned to the emission of the $\pi-\pi$ stacked aggregated forms, which is in accordance with the observation of the dimer formation in the obtained crystalline structures.[31] The phosphorescence quantum yields have moderate values up to 12%, and the corresponding lifetimes are of hundreds of nanoseconds (Table 3), in agreement with triplet state origin emission. It can be observed that the quantum yields of **series 1** in the solid state are larger than those in solution, while in the case of **series 2**, these values are in the same order as previously recorded in dichloromethane. This can be rationalized to the more efficient

https://doi.org/10.1021/acs.inorgchem.2c03490
Inorg. Chem. XXXX, XXX, XXX−XXX

Table 3. Electronic Absorption and Emission Data Including Absorption and Emission Maxima and Phosphorescence Quantum Yields Recorded in the Solid State (Powder)

compound	λ_{em}^{max} (nm)	ϕ_{Ph}	τ (μs)	k_r (μs^{-1})	k_{nr} (μs^{-1})
L1	357	0.005			
L2	390	0.008			
1	559	0.034	0.694	0.049	1.392
2	506	0.017	0.489	0.035	2.010
1a	612	0.137	0.392	0.349	2.202
1b	611	0.092	0.519	0.177	1.750
1c	601	0.049	0.593	0.083	1.604
1d	610	0.104	0.594	0.175	1.508
1e	609	0.119	0.714	0.167	1.234
2a	626	0.029	0.403	0.072	2.409
2b	617	0.058	0.339	0.171	2.779
2c	616	0.039	0.675	0.058	1.424
2d	625	0.125	0.419	0.298	2.088
2e	623	0.019	0.311	0.061	3.154

intermolecular packing in the absence of the fluoride atom at the cyclometallated ligand that seems to favor the $\pi-\pi$ stacking and the formation of aggregates, as previously observed in the packing in the X-ray diffraction determined structures. Interestingly, the calculated k_r and k_{nr} values show an enhancement of the radiative deactivation channels, with k_r values being larger in both series **1** and **2** complexes and k_{nr} values being smaller than (**1**, **1a**−**e**) or similar to (**2**, **2a**−**e**) those previously obtained in air-equilibrated solution samples.

DFT Calculations. *Geometry Optimizations.* Density functional theory (DFT) calculations in solution, using the B3LYP functional, 6-31G*/LANL2DZ basis set, and CPCM solvation model (see the Experimental Section for details), were performed on the systems **1**, **2**, **1a**-**1e**, and **2a**-**2e** in order to rationalize the experimental results. Initially, the molecular geometries of the complexes in dichloromethane were optimized. In all cases, the experimental geometries are well reproduced, with the aromatic group nearly perpendicular to the cyclometallated moiety: torsion angles are 80.5° for **1e** and 75.2° for **2c,** matching well with the experimentally determined values of 85.3 and 83.3, respectively (Figure S39 and Table S3).

We have also studied the rotation of the phenanthrenyl moiety of complex **1e**, using the same level of theory, in order to explore the possibility of the existence of rotational conformers. The calculated barrier of 3.3 kJ/mol is not high enough to preclude the free rotation around the C_{alkyne}−$C_{aromatic}$ bond.

We have analyzed the modifications in the platinum environment upon modifying the nature of the ligands. Thus, the substitution of the chlorido ligand by an aryl alkynyl moiety results in an increment of the distance between the platinum and the cyclometallated carbon and a very slight increment of the platinum−nitrogen bond length. The change of a hydrogen atom for a fluorine in the cyclometallated ligand (i.e., going from series **1** to series **2** complexes) results in a shortening of the distance between the platinum and the ligand situated in a *trans* position with respect to the metallated carbon, while the bond length between the metallated carbon and the platinum remains constant, as the one between the platinum and the nitrogen. Finally, changes in the nature of the aromatic ring bonded to the alkyne moiety only result in small variations in the distance between the alkyne carbon and the aromatic carbon bonded to it.

UV−Vis Absorption Spectra. TD-DFT calculations were performed on the systems **1**, **2**,**1a**-**1e**, and **2a**-**2e** in solution, using the geometries previously optimized, in order to calculate the ultraviolet (UV) absorption spectra using dichloromethane as a solvent. The most intense transitions are shown in Table S4. Figure S40a,b shows the energy and the nature of the orbitals involved in these transitions for complexes **1** and **1a**-**1e**, as well as the energy of the corresponding transitions. All of these transitions are of $\pi-\pi^*$ type.

Highest occupied molecular orbital−lowest unoccupied molecular orbital (HOMO−LUMO) transitions are only observable in complexes **1** and **2**. These orbitals, for complex **1**, are shown in Figure 6a; the HOMO orbital is centered mainly in the central ring of the cyclometallated moiety, with smaller contributions from the platinum atom and the chlorido ligand, while the LUMO has the greatest contribution from the N-substituted rings of the same pincer ligand, also with a small contribution of the platinum atom. This transition is ILCT/LLCT in character.

In the remaining systems, the lowest energy absorption corresponds mainly to a HOMO−1 to LUMO+1 transition. The former is based mainly on the alkyne moiety and the central ring of the cyclometallated ligand, with a very small contribution of Pt, while the latter is based mainly on the three rings of the same ligand, as shown in Figure 6b for complex **1a**. Thus, this transition is ILCT/LLCT in character.

Complexes **1a**-**1e** and **2a**-**2e** show an absorption band in the 380−390 nm interval. We have assigned it to a HOMO−1 - > LUMO transition. As previously stated, HOMO−1 has a contribution of the alkyne moiety and the central ring of the cyclometallated ligand, while LUMO is centered on the N-substituted rings of the pincer ligand; thus, this transition is also ILCT/LLCT in character. Figure 6c shows these orbitals for the **1c** complex.

Systems with naphthyl (**1d** and **2d**) and phenanthrenyl (**1e** and **2e**) substituents also feature a band in the 309−319 nm interval. There are several transitions that can contribute to this band, but the one that is always present is HOMO−3→ LUMO+1 (HOMO−3→ LUMO in **2e**). Both orbitals are centered in the pincer ligand, as shown in Figure 6d for the **1d** complex, so this transition can be regarded as ILCT.

Finally, complexes **1e** and **2e** feature a supplementary absorption band at 333−334 nm, which can be ascribed to the HOMO → LUMO+2 transition. Both orbitals are centered mainly in the phenanthrenyl moiety, as shown in Figure 6e for complex **1e**, so this transition can also be regarded as ILCT.

Emission Spectra. The triplet excited states for molecules **1**, **2**, **1a**-**1e**, and **2a**-**2e** have been optimized in solution in order to study their emission spectra, and the singlet−triplet transitions have been calculated using dichloromethane as a solvent. The transitions are listed in Table S5. The optimized geometries differ from the ground state in the orientation of the ring attached to the alkyne moiety: while in the ground state, the ring is nearly perpendicular to the cyclometallated moiety, in the triplet state, they are nearly coplanar.

The transition corresponds in nearly all the cases to a LUMO+1→ HOMO transition. The former is centered in the alkynyl-R_2 moiety, while the latter is centered in the cyclometallated ligand with some contribution of the metal for metal complexes; thus, this transition can be assigned to present a mixed ILCT/LLCT/MLCT character in nature. On

https://doi.org/10.1021/acs.inorgchem.2c03490
Inorg. Chem. XXXX, XXX, XXX−XXX

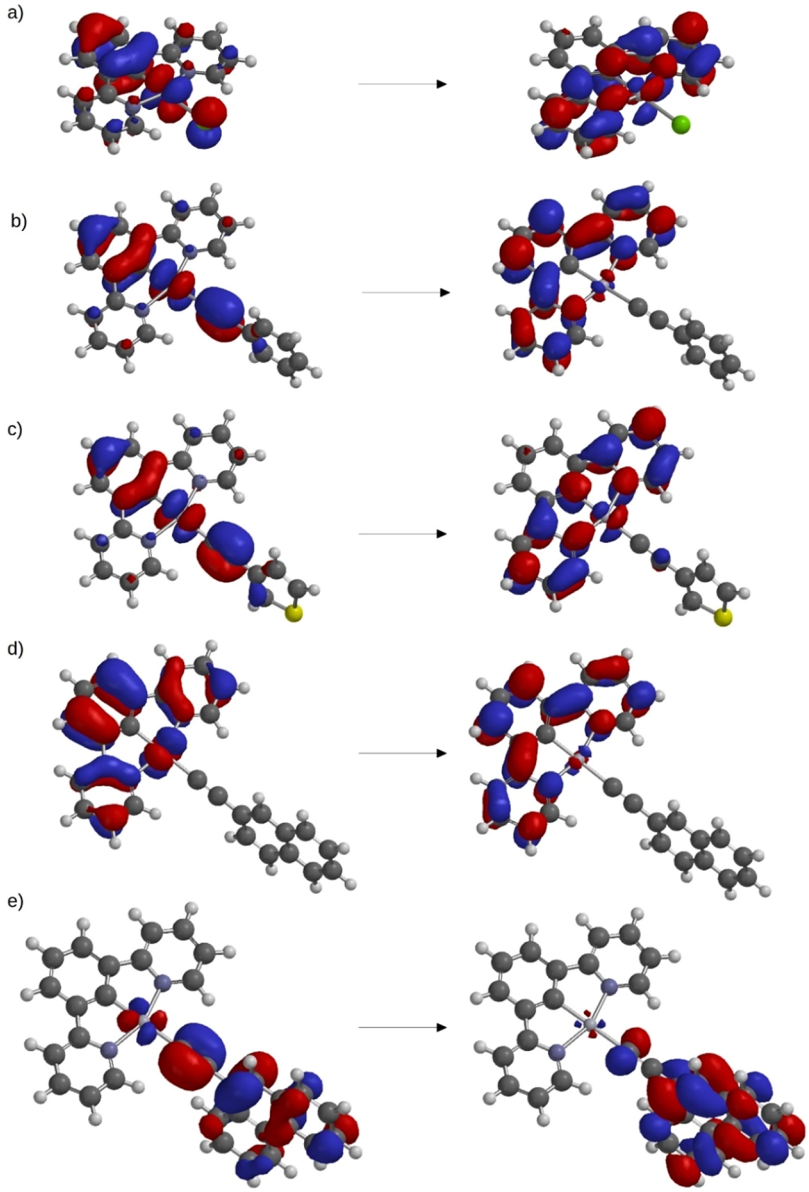

Figure 6. Orbitals that are involved in the transitions described in the text. (a) HOMO and LUMO of complex **1**; (b) HOMO−1 and LUMO+1 of complex **1a**; (c) HOMO−1 and LUMO of complex **1c**; (d) HOMO−3 and LUMO+1 of complex **1d**; and (e) HOMO and LUMO+2 of complex **1e**.

the other hand, **1e** has a contribution from HOMO−LUMO and HOMO to LUMO−2 transitions. In this case, the HOMO is again based mainly in the alkynyl-R_2 moiety, and the LUMO is centered in the cyclometallated ligand, so it corresponds to the LUMO+1 orbital of the remaining systems. The LUMO+2 orbital, in contrast, is centered mainly in the phenanthrenyl moiety. As an example, Figure S41 shows the orbitals LUMO +1 and HOMO that take part in this transition for complex **1a**.

Aggregation-Induced Emission (AIE) Experiments. To try to induce the red-shifted emission in air-equilibrated samples, water was tested as a bad solvent to induce aggregation by preparing several acetonitrile/water mixtures. The absorption spectra of the compounds in acetonitrile and 90%:10% water/acetonitrile (Figure S42) show a change in the absorption band that presents a shoulder shifted at higher wavelengths. This suggests that upon the addition of water, new aggregated species is formed, which is present in the ground state.

The resulting behavior is observed to be strongly dependent on the alkynyl-R_2 group. In general, the formation of a new band around 650 nm due to the formation of emissive aggregates can be observed. The assignment of this emission band to the excimer in acetonitrile is discarded since the latter appears at ca. 700 nm, as evidenced upon deoxygenation of the acetonitrile samples (Figure S43). Excitation spectra also support this assignment since they display a different profile from the recorded one for the monomer (Figure S44).

The AIE band is enhanced when the percentage of water is higher than 75% (Figures 7, 8, and S45). At 90% water content, its emission reaches the maximum intensity, and, in some cases, it is predominant to the monomer, even becoming the sole emission in compound **2e** affording a completely red-shifted emission. In fact, AIE seems to be more favored in **series 2** complexes (Figure 8A,B) probably due to the presence of the fluoro substituent that can establish additional intermolecular contacts, favoring the aggregation process.

https://doi.org/10.1021/acs.inorgchem.2c03490
Inorg. Chem. XXXX, XXX, XXX−XXX

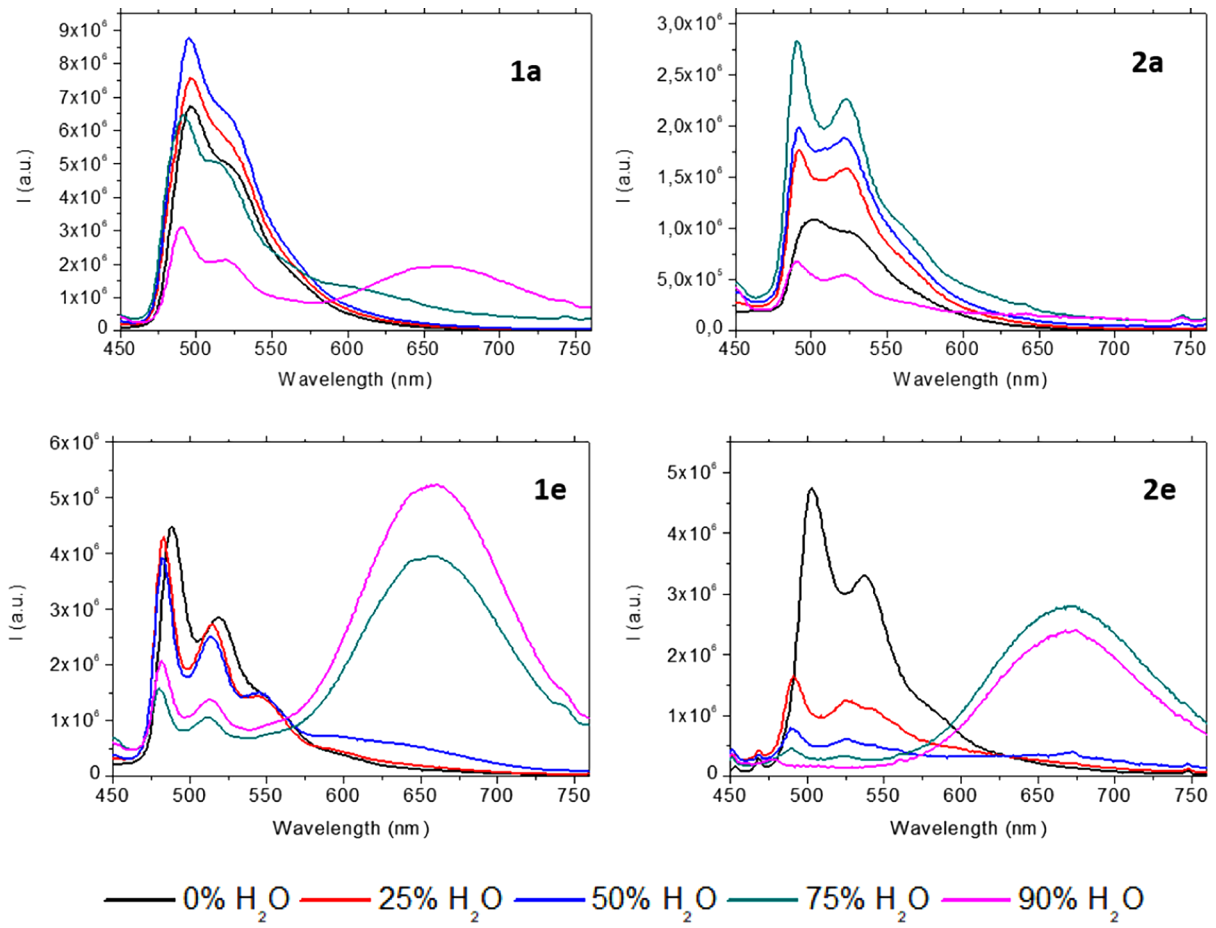

Figure 7. Emission spectra for acetonitrile/water mixtures of compounds **1a**, **1e**, **2a**, and **2e** at 298 K (λ_{exc} = 390 nm).

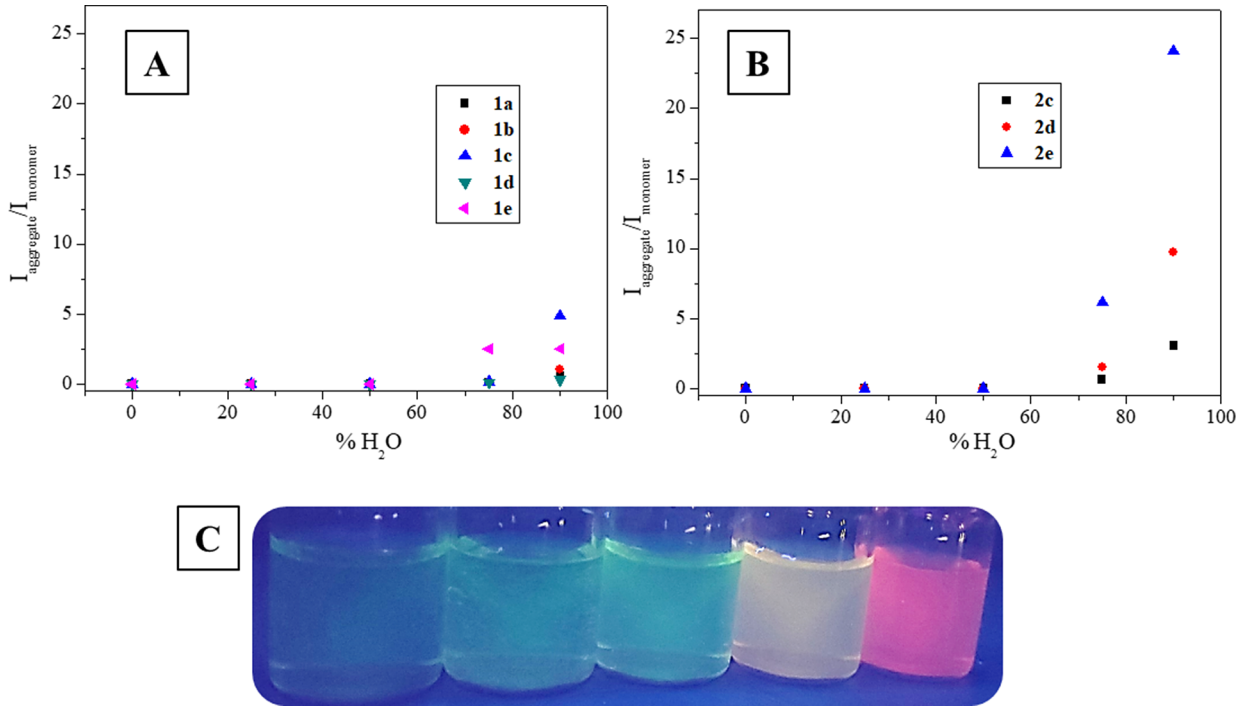

Figure 8. (A) Plot of the $I_{aggregates}/I_{monomer}$ of **series 1** complexes at different water contents (only compounds that aggregate are included in the plot). (B) Plot of the $I_{aggregates}/I_{monomer}$ of **series 2** complexes at different water contents (only compounds that aggregate are included in the plot). (C) Acetonitrile/water mixtures under the UV lamp for compound **2e** (increasing water content from left to right: 0, 25, 50, 75, and 90%).

https://doi.org/10.1021/acs.inorgchem.2c03490
Inorg. Chem. XXXX, XXX, XXX−XXX

The total phosphorescence quantum yield increases when increasing the water percentage, as expected for an AIE behavior. This is also supported by the increasing contribution of the aggregates' quantum yield when it is present by splitting the global QY value into the corresponding contributions of the monomer and the aggregated forms. The phosphorescence lifetime values of both monomer and aggregates become larger with increasing water content in all compounds, and, in all cases, $\tau_{monomer} > \tau_{aggregates}$ (Table S6).

It can be observed that the non-radiative deactivation processes are more favored in both the monomer and the aggregates in agreement with the calculated k_r and k_{nr} values (Tables S7 and S8). Additionally, the more efficient AIE effect is directly related to the k_r rate constant. In the case of the aggregates, AIE behavior is directly related to an increase of k_r rate constants. A significant increase of k_r is detected (up to 5-fold in **series 1** and more than one order of magnitude in **series 2**) in the emission of the aggregates, while the contribution of k_{nr} is much less important. That is, the aggregation processes induced by the addition of water in the acetonitrile solutions favor the intermolecular contacts and the close distance between the molecules, making the environment more rigid and favoring the efficiency of the radiative emission process as it is evidenced in the increase of the k_r constants.

■ CONCLUSIONS

N^C^N Pt(II)-cyclometallated compounds are emissive in both the solution and solid state with different emission origins. Room temperature phosphorescence emission is extremely favored in agreement with the recorded large Stokes shifts and long lifetimes. The presence of IR emission bands can be modulated by various methodologies including the formation of excimers and AIE to produce red-shifted emissions, where AIE can be favored by using a mixture of good and bad solvents, and excimer formation can be directly obtained in a homogeneous solution and the solid state (powder).

■ EXPERIMENTAL SECTION

General. Electrospray mass spectra were obtained at the Unitat d'Espectrometria de Masses (Universitat de Barcelona) in an LC/MSD-TOF spectrometer using H_2O-CH_3CN 1:1 to introduce the sample. IR spectra were recorded in KBr dispersion on an FT-IR 520 Nicolet spectrophotometer. NMR spectra were recorded in $CDCl_3$ at the Unitat d'RMN of the Universitat de Barcelona with a Mercury 400 spectrometer (^{1}H, 400 MHz; ^{19}F, 376.5 MHz). Chemical shifts are given in δ values (ppm) relative to tetramethylsilane (^{1}H) or $CFCl_3$ (^{19}F), and coupling constants J are given in Hz. Multiplicity is expressed as s (singlet), d (doublet), t (triplet), q (quadruplet), qi (quintuplet), and m (multiplet). Numbering schemes for the characterized compounds are displayed in Scheme 1.

UV−vis spectra were recorded in CH_2Cl_2 with a Cary 100 scan 388 Varian UV spectrometer. Emission and excitation spectra were recorded in a Horiba Jobin-Yvon SPEX Nanolog-TM spectrofluorometer at 298 K using 5 ×10^{-5} M solutions and in the solid state.

Emission quantum yields were determined with a Hamamatsu Quantaurus QY absolute photoluminescence quantum yield spectrometer C11347.

Luminescence lifetimes were measured on a JYF-DELTAPRO-NL equipment upon excitation of the samples with a 390 nm NanoLED and collecting the decays through a cut-off filter of 450 nm.

Preparation of the Complexes. All reagents were obtained from commercial sources and used as received. Ligands 1,3-di(2-pyridyl)-benzene (**L1**) and 2,2′-(5-fluoro-1,3-phenylene)dipyridine (**L2**) and platinum compounds **1**, **1a**, and **2** were prepared as reported elsewhere.[31,42]

General procedure for the synthesis of complexes **1x** and **2x**:[31] a mixture of arylacetylene and sodium hydroxide was stirred at room temperature under an atmosphere of nitrogen for 30 min. The corresponding precursor **1** or **2** was added, and the mixture was further stirred for 24 h. The obtained solid was filtered under reduced pressure and washed with water, methanol, and hexane.

Compound (**2a**) was obtained as an orange solid from 0.025 g (0.052 mmol) of compound **2**, 0.011 g (0.104 mmol) of phenylacetylene, and 0.004 g (0.104 mmol) of sodium hydroxide. Yield: 0.017 g (61%).

^{1}H NMR ($CDCl_3$, 400 MHz): δ 9.52 [dd, 2H, ^3J(Pt-H) = 47.6, ^3J(H-H) = 5.6, ^4J(H-H) = 1.6, H^f]; 7.96 [td, 2H, ^3J(H-H) = 8.0, ^4J(H-H) = 1.6, H^d]; 7.64 [d, 2H, ^3J(H-H) = 7.6, H^{Ph}]; 7.58 [dd, 2H, ^3J(H-H) = 8.0, ^4J(H-H) = 1.1, H^c]; 7.27 [d, 2H, ^3J(F-H) = 10.8, H^b]; 7.23−7.26 [m, 4H, H^{e,Ph}]; 7.19 [t, 1H, ^3J(H-H) = 7.6, H^{Ph}]. ^{19}F NMR ($CDCl_3$, 376.5 MHz): δ −118.62 [t, 1H, ^3J(H-F) = 9.9]. MS-ESI$^+$: m/z 989.13 [2M-C_8H_5]$^+$, 546.09 [M + H]$^+$, 444.05 [M-C_8H_5]$^+$. IR: ν 2085.34 (C≡C).

Compound (**1b**) was obtained as an orange solid from 0.020 g (0.043 mmol) of compound **1**, 0.010 g (0.086 mmol) of 1-ethynyl-4-fluorobenzene, and 0.004 g (0.086 mmol) of sodium hydroxide. Yield: 0.017 g (71%).

^{1}H NMR ($CDCl_3$, 400 MHz): δ 9.49 [d, 2H, ^3J(Pt-H) = 47.6, ^3J(H-H) = 5.5, H^f]; 7.93 [td, 2H, ^3J(H-H) = 7.8, ^4J(H-H) = 1.4, H^d]; 7.69 [d, 2H, ^3J(H-H) = 7.8, H^c]; 7.51−7.56 [m, 4H, H$^{b,Ph-F}$]; 7.24−7.26 [m, 3H, H^{a,e}]; 6.97 [t, 1H, ^3J(F-H) = ^3J(H-H) = 8.8, H^{Ph-F}]. ^{19}F NMR ($CDCl_3$, 376.5 MHz): δ −116.03 [m, 1F]. MS-ESI$^+$: m/z 971.14 [2M-C_8H_4F]$^+$, 546.09 [M + H]$^+$, 426.06 [M-C_8H_4F]$^+$. IR: ν 2081.07 (C≡C).

Compound (**2b**) was obtained as an orange solid from 0.020 g (0.042 mmol) of compound **2**, 0.010 g (0.084 mmol) of 1-ethynyl-4-fluorobenzene, and 0.003 g (0.084 mmol) of sodium hydroxide. Yield: 0.013 g (54%).

^{1}H NMR ($CDCl_3$, 400 MHz): δ 9.50 [d, 2H, ^3J(Pt-H) = 48.0, ^3J(H-H) = 5.5, H^f]; 7.97 [td, 2H, ^3J(H-H) = 7.9, ^4J(H-H) = 1.2, H^d]; 7.65 [d, 2H, ^3J(H-H) = 7.7, H^c]; 7.53 [dd, 2H, ^3J(H-H) = 8.5, ^4J(F-H) = 5.6, H^{Ph-F}]; 7.28 [d, 2H, ^3J(F-H) = 10.1, H^b]; 7.24−7.26 [m, 2H, H^e]; 6.97 [t, 1H, ^3J(F-H) = ^3J(H-H) = 8.9, H^{Ph-F}]. ^{19}F NMR ($CDCl_3$, 376.5 MHz): δ −115.88 [m, 1F], −118.14 [t, 1F, ^3J(H-F) = 10.0]. MS-ESI$^+$: m/z 1007.12 [2M-C_8H_4F]$^+$, 564.08 [M + H]$^+$, 444.05 [M-C_8H_4F]$^+$. IR: ν 2085.34 (C≡C).

Compound (**1c**) was obtained as an orange solid from 0.020 g (0.043 mmol) of compound **1**, 0.009 g (0.086 mmol) of 3-ethynylthiophene, and 0.004 g (0.086 mmol) of sodium hydroxide. Yield: 0.014 g (61%).

^{1}H NMR ($CDCl_3$, 400 MHz): δ 9.50 [dd, 2H, ^3J(Pt-H) = 47.6, ^3J(H-H) = 5.7, ^4J(H-H) = 1.6, H^f]; 7.93 [td, 2H, ^3J(H-H) = 7.6, ^4J(H-H) = 1.6, H^d]; 7.68 [d, 2H, ^3J(H-H) = 8.0, H^c]; 7.52 [d, 2H, ^3J(H-H) = 7.7, H^b]; 7.36 [dd, 1H, ^3J(H-H) = 2.8, ^4J(H-H) = 1.3, H^{Thio}]; 7.18−7.26 [m, 5H, H^{a,e,Thio}]. MS-ESI$^+$: m/z 959.11 [2M-C_6H_3S]$^+$, 534.06 [M + H]$^+$, 426.06 [M-C_6H_3S]$^+$. IR: ν 2076.81 (C≡C).

Compound (**2c**) was obtained as an orange solid from 0.020 g (0.042 mmol) of compound **2**, 0.009 g (0.084 mmol) of 3-ethynylthiophene, and 0.003 g (0.084 mmol) of sodium hydroxide. Yield: 0.015 g (65%).

^{1}H NMR ($CDCl_3$, 400 MHz): δ 9.51 [dd, 2H, ^3J(Pt-H) = 48.4, ^3J(H-H) = 5.6, ^4J(H-H) = 1.6, H^f]; 7.96 [td, 2H, ^3J(H-H) = 7.8, ^4J(H-H) = 1.7, H^d]; 7.64 [d, 2H, ^3J(H-H) = 7.9, H^c]; 7.36 [dd, 1H, ^3J(H-H) = 2.6, ^4J(H-H) = 1.5, H^{Thio}]; 7.28 [d, 2H, ^3J(F-H) = 10.1, H^b]; 7.21−7.25 [m, 4H, H^{e,Thio}]. ^{19}F NMR ($CDCl_3$, 376.5 MHz): δ −118.47 [t, 1H, ^3J(H-F) = 10.0]. MS-ESI$^+$: m/z 995.09 [2M-C_6H_3S]$^+$, 552.05 [M + H]$^+$, 444.05 [M-C_6H_3S]$^+$ IR: ν 2081.07 (C≡C).

Compound (**1d**) was obtained as an orange solid from 0.020 g (0.043 mmol) of compound **1**, 0.013 g (0.086 mmol) of 2-ethynylnaphthalene, and 0.004 g (0.086 mmol) of sodium hydroxide. Yield: 0.020 g (80%).

https://doi.org/10.1021/acs.inorgchem.2c03490
Inorg. Chem. XXXX, XXX, XXX−XXX

^{1}H NMR ($CDCl_3$, 400 MHz): δ 9.56 [dd, 2H, ^3J(Pt-H) = 47.2, ^3J(H-H) = 5.7, ^4J(H-H) = 1.5, H^f]; 8.05 [s, 1H, H^{Naph}]; 7.94 [td, 2H, ^3J(H-H) = 7.8, ^4J(H-H) = 1.6, H^d], 7.73−7.81 [m, 3H, H^{Naph}]; 7.67−7.72 [m, 3H, $H^{c,Naph}$], 7.54 [d, 2H, ^3J(H-H) = 7.7, H^b]; 7.34−7.46 [m, 2H, H^{Naph}]; 7.21−7.26 [m, 3H, $H^{a,e}$]. **MS-ESI$^+$**: m/z 1003.16 [2M-$C_{12}H_7$]$^+$, 578.12 [M + H]$^+$, 426.06 [M-$C_{12}H_7$]$^+$. **IR**: ν 2085.34 (C≡C).

Compound (**2d**) was obtained as an orange solid from 0.015 g (0.033 mmol) of compound **2**, 0.010 g (0.066 mmol) of 2-ethynylnaphthalene, and 0.003 g (0.066 mmol) of sodium hydroxide. Yield: 0.012 g (61%).

^{1}H NMR ($CDCl_3$, 400 MHz): δ 9.57 [dd, 2H, ^3J(Pt-H) = 48.0, ^3J(H-H) = 5.7, ^4J(H-H) = 1.5, H^f]; 8.05 [s, 1H, H^{Naph}]; 7.98 [td, 2H, ^3J(H-H) = 7.8, ^4J(H-H) = 1.6, H^d], 7.77−7.79 [m, 3H, H^{Naph}]; 7.66−7.68 [m, 3H, $H^{c,Naph}$]; 7.42 [m, 2H, H^{Naph}]; 7.29 [d, 2H, ^3J(F-H) = 10.0, H^b]; 7.26−7.29 [m, 2H, H^e]. ^{19}F NMR ($CDCl_3$, 376.5 MHz): δ −118.47 [t, 1H, ^3J(H-F) = 10.0]. MS-ESI$^+$: m/z 10039.15 [2M-$C_{12}H_7$]$^+$, 596.11 [M + H]$^+$, 444.05 [M-$C_{12}H_7$]$^+$. IR: ν 2085.34 (C≡C).

Compound (**1e**) was obtained as an orange solid from 0.020 g (0.043 mmol) of compound **1**, 0.017 g (0.086 mmol) of 9-ethynylphenanthrene, and 0.004 g (0.086 mmol) of sodium hydroxide. Yield: 0.017 g (63%).

^{1}H NMR ($CDCl_3$, 400 MHz): δ 9.63 [dd, 2H, ^3J(Pt-H) = 48.0, ^3J(H-H) = 5.7, ^4J(H-H) = 1.6, H^f]; 8.98 [m, 1H, H^{Phen}]; 8.71 [m, 1H, H^{Phen}]; 8.65 [d, 1H, ^3J(H-H) = 7.9, H^{Phen}]; 8.08 [s, 1H, H^{Phen}]; 7.95 [td, 2H, ^3J(H-H) = 7.8, ^4J(H-H) = 1.6, H^d], 7.84 [dd, 1H, ^3J(H-H) = 7.6, ^4J(H-H) = 1.6, H^{Phen}], 7.72 [d, 2H, ^3J(H-H) = 7.8, H^c]; 7.66 [m, 2H, H^{Phen}]; 7.53−7.61 [m, 3H, $H^{b,Phen}$]; 7.19−7.25 [m, 3H, $H^{a,e}$]. MS-ESI$^+$: m/z 1053.18 [2M-$C_{16}H_9$]$^+$, 628.14 [M + H]$^+$, 426.06 [M-$C_{16}H_9$]$^+$. IR: ν 2064.01 (C≡C).

Compound (**2e**) was obtained as an orange solid from 0.020 g (0.042 mmol) of compound **2**, 0.017 g (0.084 mmol) of 9-ethynylphenanthrene, and 0.004 g (0.084 mmol) of sodium hydroxide. Yield: 0.020 g (74%).

^{1}H NMR ($CDCl_3$, 400 MHz): δ 9.64 [dd, 2H, ^3J(Pt-H) = 48.4, ^3J(H-H) = 5.7, ^4J(H-H) = 1.5, H^f]; 8.97 [m, 1H, H^{Phen}]; 8.71 [m, 1H, H^{Phen}]; 8.65 [d, 1H, ^3J(H-H) = 7.9, H^{Phen}]; 8.08 [s, 1H, H^{Phen}]; 7.98 [td, 2H, ^3J(H-H) = 7.8, ^4J(H-H) = 1.6, H^d], 7.84 [dd, 1H, ^3J(H-H) = 7.3, ^4J(H-H) = 2.0, H^{Phen}], 7.67 [m, 4H, $H^{c,Phen}$]; 7.57 [m, 2H, H^{Phen}]; 7.31 [d, 2H, ^3J(F-H) = 10.0, H^b]; 7.24−7.28 [m, 2H, H^e]. ^{19}F NMR ($CDCl_3$, 376.5 MHz): δ −118.35 [t, 1H, ^3J(H-F) = 10.0]. MS-ESI$^+$: m/z 1089.16 [2M-$C_{16}H_9$]$^+$, 646.12 [M + H]$^+$, 444.05 [M-$C_{16}H_9$]$^+$. IR: ν 2072.54 (C≡C).

X-ray Diffraction. Single crystals suitable for X-ray diffraction analysis were grown for **1e** and **2c** by slow diffusion of methanol or hexane, respectively, in a dichloromethane solution of the compounds.

Single-crystal X-ray data for **1e** and **2c** were obtained using a Bruker-Nonius Kappa CCD diffractometer with an APEX-II detector with graphite-monochromatized Mo Kα (λ = 0.71073 Å) radiation. Data collection and reduction were performed using the program *COLLECT*[43] and *HKL DENZO AND SCALEPACK*,[44] respectively, and the intensities were corrected for absorption using *SADABS*.[45] The structures were solved with intrinsic phasing (*SHELXT*)[46] and refined by full-matrix least squares on F^2 using the *OLEX2* software,[47] which utilizes the *SHELXL* module.[48]

■ COMPUTATIONAL DETAILS

Theoretical calculations were performed at the DFT level using Q-chem 5.1,[49] included in Spartan 20.[50] The functional chosen was B3LYP,[51] and the basis set was chosen as follows: 6-31G* for C, H, N, and Cl, including polarization functions for non-hydrogen atoms,[52] and LANL2DZ[53] for Pt. Solvent effects were considered using the CPCM model.[54] No symmetry restrictions were imposed. Optimized geometries are given in Table S9.

■ ASSOCIATED CONTENT

Supporting Information

The Supporting Information is available free of charge at https://pubs.acs.org/doi/10.1021/acs.inorgchem.2c03490.

Characterization data of the compounds; X-ray packing images of **1e** and **2c**; absorption, emission, and excitation spectra of the compounds in dichloromethane and in the solid state; absorption, emission, and excitation spectra of the compounds in acetonitrile/water mixtures; DFT optimized geometries in solution of the compounds; orbitals that participate in the UV−vis transitions; crystal data and structure refinement tables; radiative and non-radiative rate constants obtained in air-equilibrated (with O_2) or degassed (N_2 sat.) dichloromethane and acetonitrile/water solutions; phosphorescence quantum yields and lifetimes recorded in aerated acetonitrile/water mixtures; key geometrical parameters optimized at the DFT level in solution; and experimental and calculated UV−vis and emission transitions (PDF)

Accession Codes

CCDC 2192597−2192598 contain the supplementary crystallographic data for this paper. These data can be obtained free of charge via www.ccdc.cam.ac.uk/data_request/cif, or by emailing data_request@ccdc.cam.ac.uk, or by contacting The Cambridge Crystallographic Data Centre, 12 Union Road, Cambridge CB2 1EZ, UK; fax: +44 1223 336033.

■ AUTHOR INFORMATION

Corresponding Author

Laura Rodríguez − *Departament de Química Inorgànica i Orgànica, Secció de Química Inorgànica, Universitat de Barcelona, E-08028 Barcelona, Spain; Institut de Nanociència i Nanotecnologia (IN2UB), Universitat de Barcelona, 08028 Barcelona, Spain;* orcid.org/0000-0003-1289-1587; Email: laura.rodriguez@qi.ub.es

Authors

Ariadna Lázaro − *Departament de Química Inorgànica i Orgànica, Secció de Química Inorgànica, Universitat de Barcelona, E-08028 Barcelona, Spain; Institut de Nanociència i Nanotecnologia (IN2UB), Universitat de Barcelona, 08028 Barcelona, Spain*

Ramon Bosque − *Departament de Química Inorgànica i Orgànica, Secció de Química Inorgànica, Universitat de Barcelona, E-08028 Barcelona, Spain*

Jas S. Ward − *Department of Chemistry, University of Jyvaskyla, 40014 Jyväskylä, Finland;* orcid.org/0000-0001-9089-9643

Kari Rissanen − *Department of Chemistry, University of Jyvaskyla, 40014 Jyväskylä, Finland;* orcid.org/0000-0002-7282-8419

Margarita Crespo − *Departament de Química Inorgànica i Orgànica, Secció de Química Inorgànica, Universitat de Barcelona, E-08028 Barcelona, Spain; Institut de Biomedicina de la Universitat de Barcelona (IBUB), 08028 Barcelona, Spain;* orcid.org/0000-0002-7086-9751

Complete contact information is available at: https://pubs.acs.org/10.1021/acs.inorgchem.2c03490

Notes

The authors declare no competing financial interest.

■ ACKNOWLEDGMENTS

The authors acknowledge Project PID2019-104121GB-I00 funded by the Ministerio de Ciencia e Innovación of Spain (MCIN/AEI/10.13039/501100011033), the Magnus Ehrnrooth Foundation (J.S.W.), and the Academy of Finland (K.R., grant no. 317259) for funding.

■ REFERENCES

(1) Yam, V. W.-W.; Law, A. S.-Y. Luminescent D8 Metal Complexes of Platinum(II) and Gold(III): From Photophysics to Photofunctional Materials and Probes. *Coord. Chem. Rev.* **2020**, *414*, No. 213298.

(2) Goswami, S.; Winkel, R. W.; Schanze, K. S. Photophysics and Nonlinear Absorption of Gold(I) and Platinum(II) Donor−Acceptor−Donor Chromophores. *Inorg. Chem.* **2015**, *54*, 10007−10014.

(3) Nisic, F.; Colombo, A.; Dragonetti, C.; Roberto, D.; Valore, A.; Malicka, J. M.; Cocchi, M.; Freeman, G. R.; Williams, J. A. G. Platinum(II) Complexes with Cyclometallated 5-π-Delocalized-Donor-1,3- Di(2-Pyridyl)Benzene Ligands as Efficient Phosphors for NIR-OLEDs. *J. Mater. Chem. C* **2014**, *2*, 1791−1800.

(4) Lázaro, A.; Cunha, C.; Bosque, R.; Pina, J.; Ward, J. S.; Truong, K.-N.; Rissanen, K.; Lima, J. C.; Crespo, M.; Seixas de Melo, J. S.; Rodríguez, L. Room-Temperature Phosphorescence and Efficient Singlet Oxygen Production by Cyclometalated Pt(II) Complexes with Aromatic Alkynyl Ligands. *Inorg. Chem.* **2020**, *59*, 8220−8230.

(5) Lázaro, A.; Balcells, C.; Quirante, J.; Badia, J.; Baldomà, L.; Ward, J. S.; Rissanen, K.; Font-Bardia, M.; Rodríguez, L.; Crespo, M.; Cascante, M. Luminescent Pt II and Pt IV Platinacycles with Anticancer Activity Against Multiplatinum-Resistant Metastatic CRC and CRPC Cell Models. *Chem. − Eur. J.* **2020**, *26*, 1947−1952.

(6) Lázaro, A.; Serra, O.; Rodríguez, L.; Crespo, M.; Font-Bardia, M. Luminescence Studies of New [C,N,N′] Cyclometallated Platinum(II) and Platinum(IV) Compounds. *New J. Chem.* **2019**, *43*, 1247−1256.

(7) Martínez-Junquera, M.; Lara, R.; Lalinde, E.; Moreno, M. T. Isomerism, Aggregation-Induced Emission and Mechanochromism of Isocyanide Cycloplatinated(II) Complexes. *J. Mater. Chem. C* **2020**, *8*, 7221−7233.

(8) Fang, B.; Zhu, Y.; Hu, L.; Shen, Y.; Jiang, G.; Zhang, Q.; Tian, X.; Li, S.; Zhou, H.; Wu, J.; Tian, Y. Series of C^N^C Cyclometalated Pt(II) Complexes: Synthesis, Crystal Structures, and Nonlinear Optical Properties in the Near-Infrared Region. *Inorg. Chem.* **2018**, *57*, 14134−14143.

(9) Hruzd, M.; Gauthier, S.; Boixel, J.; Kahlal, S.; le Poul, N.; Saillard, J. Y.; Achelle, S.; le Guen, F. R. N^N^C Platinum (II) Complexes Based on Phenyl-Pyridin-2-Ylpyrimidine Ligands: Synthesis, Electrochemical and Photophysical Properties. *Dyes Pigm.* **2021**, *194*, No. 109622.

(10) Guo, Z.; Chan, M. C. W. Shape-Persistent Binuclear Cyclometalated Platinum(II) Luminophores: Pushing π-Mediated Excimeric Fluid Emissions into the NIR Region and Ion-Induced Perturbations. *Chem. − Eur. J.* **2009**, *15*, 12585−12588.

(11) Pinter, P.; Soellner, J.; Strassner, T. Metallophilic Interactions in Bimetallic Cyclometalated Platinum(II) N-Heterocyclic Carbene Complexes. *Eur. J. Inorg. Chem.* **2021**, *2021*, 3104−3107.

(12) Zhao, S.; Zhu, Y.; Li, L.; Guerchais, V.; Boixel, J.; Wong, K. M.-C. The Switchable Phosphorescence and Delayed Fluorescence of a New Rhodamine-like Dye through Allenylidene Formation in a Cyclometallated Platinum(II) System. *Chem. Sci.* **2021**, *12*, 11056−11064.

(13) Rogers, J. E.; Slagle, J. E.; Krein, D. M.; Burke, A. R.; Hall, B. C.; Fratini, A.; McLean, D. G.; Fleitz, P. A.; Cooper, T. M.; Drobizhev, M.; Makarov, N. S.; Rebane, A.; Kim, K.-Y.; Farley, R.; Schanze, K. S. Platinum Acetylide Two-Photon Chromophores. *Inorg. Chem.* **2007**, *46*, 6483−6494.

(14) Kalinowski, J.; Fattori, V.; Cocchi, M.; Williams, J. A. G. Light-Emitting Devices Based on Organometallic Platinum Complexes as Emitters. *Coord. Chem. Rev.* **2011**, *255*, 2401−2425.

(15) Yam, V. W.-W.; Au, V. K.-M.; Leung, S. Y.-L. Light-Emitting Self-Assembled Materials Based on d 8 and d 10 Transition Metal Complexes. *Chem. Rev.* **2015**, *115*, 7589−7728.

(16) Chan, A. K. W.; Ng, M.; Wong, Y. C.; Chan, M. Y.; Wong, W. T.; Yam, V. W. W. Synthesis and Characterization of Luminescent Cyclometalated Platinum(II) Complexes with Tunable Emissive Colors and Studies of Their Application in Organic Memories and Organic Light-Emitting Devices. *J. Am. Chem. Soc.* **2017**, *139*, 10750−10761.

(17) Gareth Williams, J. A.; Develay, S.; Rochester, D. L.; Murphy, L. Optimising the Luminescence of Platinum(II) Complexes and Their Application in Organic Light Emitting Devices (OLEDs). *Coord. Chem. Rev.* **2008**, *252*, 2596−2611.

(18) Kim, D.; Brédas, J.-L. Triplet Excimer Formation in Platinum-Based Phosphors: A Theoretical Study of the Roles of Pt−Pt Bimetallic Interactions and Interligand Π−π Interactions. *J. Am. Chem. Soc.* **2009**, *131*, 11371−11380.

(19) Dragonetti, C.; Fagnani, F.; Marinotto, D.; Di Biase, A.; Roberto, D.; Cocchi, M.; Fantacci, S.; Colombo, A. First Member of an Appealing Class of Cyclometalated 1,3-Di-(2-Pyridyl)Benzene Platinum(II) Complexes for Solution-Processable OLEDs. *J. Mater. Chem. C* **2020**, *8*, 7873−7881.

(20) Sun, Y.; Yang, X.; Liu, B.; Guo, H.; Zhou, G.; Ma, W.; Wu, Z. Aggregation-Induced Emission Triggered by the Radiative-Transition-Switch of a Cyclometallated Pt(Ii) Complex. *J. Mater. Chem. C* **2019**, *7*, 12552−12559.

(21) Xiang, H.; Cheng, J.; Ma, X.; Zhou, X.; Chruma, J. J. *Near-Infrared Phosphorescence: Materials and Applications*, 2013; vol *42*.

(22) Zhao, Q.; Sun, J. Z. Red and near Infrared Emission Materials with AIE Characteristics. *J. Mater. Chem. C* **2016**, *4*, 10588−10609.

(23) Ho, C.-L.; Li, H.; Wong, W.-Y. Red to Near-Infrared Organometallic Phosphorescent Dyes for OLED Applications. *J. Organomet. Chem.* **2014**, *751*, 261−285.

(24) Sajjad, M. T.; Manousiadis, P. P.; Chun, H.; Vithanage, D. A.; Rajbhandari, S.; Kanibolotsky, A. L.; Faulkner, G.; Obrien, D.; Skabara, P. J.; Samuel, I. D. W.; Turnhbull, G. Novel Fast Color-Converter for Visible Light Communication Using a Blend of Conjugated Polymers. *ACS Photonics* **2015**, *2*, 194−199.

(25) Zampetti, A.; Minotto, A.; Cacialli, F. Near-Infrared (NIR) Organic Light-Emitting Diodes (OLEDs): Challenges and Opportunities. *Adv. Funct. Mater.* **2019**, *29*, No. 1807623.

(26) Zhao, J.; Feng, Z.; Zhong, D.; Yang, X.; Wu, Y.; Zhou, G.; Wu, Z. Cyclometalated Platinum Complexes with Aggregation-Induced Phosphorescence Emission Behavior and Highly Efficient Electroluminescent Ability. *Chem. Mater.* **2018**, *30*, 929−946.

(27) Sun, Y.; Yang, X.; Liu, B.; Guo, H.; Zhou, G.; Ma, W.; Wu, Z. Aggregation-Induced Emission Triggered by the Radiative-Transition-Switch of a Cyclometallated Pt(II) Complex. *J. Mater. Chem. C* **2019**, *7*, 12552−12559.

(28) Mróz, W.; Botta, C.; Giovanella, U.; Rossi, E.; Colombo, A.; Dragonetti, C.; Roberto, D.; Ugo, R.; Valore, A.; Williams, J. A. G. Cyclometallated Platinum(II) Complexes of 1,3-Di(2-Pyridyl)-Benzenes for Solution-Processable WOLEDs Exploiting Monomer and Excimer Phosphorescence. *J. Mater. Chem.* **2011**, *21*, 8653−8661.

(29) Pinto, A.; Echeverri, M.; Gómez-Lor, B.; Rodríguez, L. How to Achieve near Unity Fluorescence Quantum Yields on Gold(I) Benzothiadiazole-Based Derivatives. *Dyes Pigm.* **2022**, *202*, No. 110308.

(30) Cunha, C.; Pinto, A.; Galvão, A.; Rodríguez, L.; Seixas De Melo, J. S. Aggregation-Induced Emission with Alkynylcoumarin Dinuclear Gold(I) Complexes: Photophysical, Dynamic Light Scattering, and Time-Dependent Density Functional Theory Studies. *Inorg. Chem.* **2022**, *61*, 6964−6976.

(31) Chen, Y.; Li, K.; Lu, W.; Chui, S. S.-Y.; Ma, C.-W.; Che, C.-M. Photoresponsive Supramolecular Organometallic Nanosheets Induced by PtII···PtII and C-H···π Interactions. *Angew. Chem., Int. Ed.* **2009**, *48*, 9909−9913.

(32) Lu, W.; Mi, B. X.; Chan, M. C. W.; Hui, Z.; Che, C. M.; Zhu, N.; Lee, S. T. Light-Emitting Tridentate Cyclometalated Platinum(II)

https://doi.org/10.1021/acs.inorgchem.2c03490
Inorg. Chem. XXXX, XXX, XXX−XXX

Complexes Containing σ-Alkynyl Auxiliaries: Tuning of Photo- and Electrophosphorescence. *J. Am. Chem. Soc.* **2004**, *126*, 4958−4971.

(33) Cheng, G.; Chen, Y.; Yang, C.; Lu, W.; Che, C. M. Highly Efficient Solution-Processable Organic Light-Emitting Devices with Pincer-Type Cyclometalated Platinum(II) Arylacetylide Complexes. *Chem. − Asian J.* **2013**, *8*, 1754−1759.

(34) Baik, C.; Han, W. S.; Kang, Y.; Kang, S. O.; Ko, J. Synthesis and Photophysical Properties of Luminescent Platinum(II) Complexes with Terdentate Polypyridine Ligands: [Pt(Bpqb)X] and [Pt(Tbbpqpy)X](PF6) (Bpqb-H = 1,3-Bis(4′-Phenyl-2′-Quinolinyl) Benzene; Tbbpqpy = 4-Tert-Butyl-1,3-Bis(4′-Phenyl-2′-Quinolinyl) Pyridine. *J. Organomet. Chem.* **2006**, *691*, 5900−5910.

(35) Yang, S.; Meng, F.; Wu, X.; Yin, Z.; Liu, X.; You, C.; Wang, Y.; Su, S.; Zhu, W. Dinuclear Platinum(Ii) Complex Dominated by a Zig-Zag-Type Cyclometalated Ligand: A New Approach to Realize High-Efficiency near Infrared Emission. *J. Mater. Chem. C* **2018**, *6*, 5769−5777.

(36) Zhang, H.-H.; Wu, S.-X.; Wang, Y.-Q.; Xie, T.-G.; Sun, S.-S.; Liu, Y.-L.; Han, L.-Z.; Zhang, X.-P.; Shi, Z.-F. Mechanochromic Luminescent Property and Anti-Counterfeiting Application of AIE-Active Cyclometalated Platinum(II) Complexes Featuring a Fused Five-Six-Membered Metallacycle. *Dyes Pigm.* **2022**, *197*, No. 109857.

(37) Rossi, E.; Colombo, A.; Dragonetti, C.; Roberto, D.; Ugo, R.; Valore, A.; Falciola, L.; Brulatti, P.; Cocchi, M.; Williams, J. A. G. Novel N^C^N-Cyclometallated Platinum Complexes with Acetylide Co-Ligands as Efficient Phosphors for OLEDs. *J. Mater. Chem.* **2012**, *22*, 10650−10655.

(38) Mróz, W.; Botta, C.; Giovanella, U.; Rossi, E.; Colombo, A.; Dragonetti, C.; Roberto, D.; Ugo, R.; Valore, A.; Williams, J. A. G. Cyclometallated Platinum(Ii) Complexes of 1,3-Di(2-Pyridyl)-Benzenes for Solution-Processable WOLEDs Exploiting Monomer and Excimer Phosphorescence. *J. Mater. Chem.* **2011**, *21*, 8653−8661.

(39) Williams, J. A. G.; Beeby, A.; Davies, E. S.; Weinstein, J. A.; Wilson, C. An Alternative Route to Highly Luminescent Platinum(II) Complexes: Cyclometalation with N/\C/\N-Coordinating Dipyridylbenzene Ligands. *Inorg. Chem.* **2003**, *42*, 8609−8611.

(40) Farley, S. J.; Rochester, D. L.; Thompson, A. L.; Howard, J. A. K.; Williams, J. A. G. Controlling Emission Energy, Self-Quenching, and Excimer Formation in Highly Luminescent N∧C∧N-Coordinated Platinum(II) Complexes. *Inorg. Chem.* **2005**, *44*, 9690−9703.

(41) Gong, Z. L.; Tang, K.; Zhong, Y. W. A Carbazole-Bridged Biscyclometalated Diplatinum Complex: Synthesis, Characterization, and Dual-Mode Aggregation-Enhanced Phosphorescence. *Inorg. Chem.* **2021**, *60*, 6607−6615.

(42) Wang, Z.; Turner, E.; Mahoney, V.; Madakuni, S.; Groy, T.; Li, J. Facile Synthesis and Characterization of Phosphorescent Pt(N^C^N)X Complexes. *Inorg. Chem.* **2010**, *49*, 11276−11286.

(43) Hooft, R.W.W. *COLLECT*; Nonius BV: Delft, The Netherlands, (1998).

(44) Otwinowski, Z.; Minor, W. *Methods in Enzymology, Macromolecular Crystallography, Part A*; Carter, Jr, C. W., Sweet, R. M., Eds.; Academic Press: New York, 1997, vol *276*; pp 307−326.

(45) Sheldrick, G. M. *SADABS Version 2008/2*; University of Göttingen: Germany, 1996.

(46) Sheldrick, G. M. SHELXT - Integrated space-group and crystal-structure determination. *Acta Crystallogr., Sect. A: Found. Adv.* **2015**, *A71*, 3−8.

(47) Dolomanov, O. V.; Bourhis, L. J.; Gildea, R. J.; Howard, J. A. K.; Puschmann, H. OLEX2: a complete structure solution, refinement and analysis program. *J. Appl. Crystallogr.* **2009**, *42*, 339−341.

(48) Sheldrick, G. M. Crystal structure refinement with SHELXL. *Acta Crystallogr., Sect. C: Struct. Chem.* **2015**, *C71*, 3−8.

(49) Shao, Y.; Gan, Z.; Epifanovsky, E.; Gilbert, A. T. B.; Wormit, M.; Kussmann, J.; Lange, A. W.; Behn, A.; Deng, J.; Feng, X.; Ghosh, D.; Goldey, M.; Horn, P. R.; Jacobson, L. D.; Kaliman, I.; Khaliullin, R. Z.; Kús, T.; Landau, A.; Liu, J.; Proynov, E. I.; Rhee, Y. M.; Richard, R. M.; Rohrdanz, M. A.; Steele, R. P.; Sundstrom, E. J.; Woodcock, H. L., III; Zimmerman, P. M.; Zuev, D.; Albrecht, B.; Alguire, E.; Austin, B.; Beran, G. J. O.; Bernard, Y. A.; Berquist, E.; Brandhorst, K.; Bravaya, K. B.; Brown, S. T.; Casanova, D.; Chang, C.-M.; Chen, Y.; Chien, S. H.; Closser, K. D.; Crittenden, D. L.; Diedenhofen, M.; DiStasio, R. A., Jr.; Dop, H.; Dutoi, A. D.; Edgar, R. G.; Fatehi, S.; Fusti-Molnar, L.; Ghysels, A.; Golubeva-Zadorozhnaya, A.; Gomes, J.; Hanson-Heine, M. W. D.; Harbach, P. H. P.; Hauser, A. W.; Hohenstein, E. G.; Holden, Z. C.; Jagau, T.-C.; Ji, H.; Kaduk, B.; Khistyaev, K.; Kim, J.; Kim, J.; King, R. A.; Klunzinger, P.; Kosenkov, D.; Kowalczyk, T.; Krauter, C. M.; Lao, K. U.; Laurent, A.; Lawler, K. V.; Levchenko, S. V.; Lin, C. Y.; Liu, F.; Livshits, E.; Lochan, R. C.; Luenser, A.; Manohar, P.; Manzer, S. F.; Mao, S.-P.; Mardirossian, N.; Marenich, A. V.; Maurer, S. A.; Mayhall, N. J.; Oana, C. M.; Olivares-Amaya, R.; O'Neill, D. P.; Parkhill, J. A.; Perrine, T. M.; Peverati, R.; Pieniazek, P. A.; Prociuk, A.; Rehn, D. R.; Rosta, E.; Russ, N. J.; Sergueev, N.; Sharada, S. M.; Sharmaa, S.; Small, D. W.; Sodt, A.; Stein, T.; Stück, D.; Su, Y.-C.; Thom, A. J. W.; Tsuchimochi, T.; Vogt, L.; Vydrov, O.; Wang, T.; Watson, M. A.; Wenzel, J.; White, A.; Williams, C. F.; Vanovschi, V.; Yeganeh, S.; Yost, S. R.; You, Z.-Q.; Zhang, I. Y.; Zhang, X.; Zhou, Y.; Brooks, B. R.; Chan, G. K. L.; Chipman, D. M.; Cramer, C. J.; Goddard, W. A., III; Gordon, M. S.; Hehre, W. J.; Klamt, A.; Schaefer, H. F., III; Schmidt, M. W.; Sherrill, C. D.; Truhlar, D. G.; Warshel, A.; Xua, X.; Aspuru-Guzik, A.; Baer, R.; Bell, A. T.; Besley, N. A.; Chai, J.-D.; Dreuw, A.; Dunietz, B. D.; Furlani, T. R.; Gwaltney, S. R.; Hsu, C.-P.; Jung, Y.; Kong, J.; Lambrecht, D. S.; Liang, W.; Ochsenfeld, C.; Rassolov, V. A.; Slipchenko, L. V.; Subotnik, J. E.; Van Voorhis, T.; Herbert, J. M.; Krylov, A. I.; Gill, P. M. W.; Head-Gordon, M. *Mol. Phys.* **2015**, *113*, 184−215.

(50) *Spartan'20*; Wavefunction, Inc.: Irvine, CA.

(51) (a) Becke, A. D. Density-functional thermochemistry. III. The role of exact Exchange. *J. Chem. Phys.* **1993**, *98*, 5648−5652. (b) Lee, C.; Yang, W.; Parr, R. G. Development of the Colle-Salvetti correlation-energy formula into a functional of the electron density. *Phys. Rev. B: Condens. Matter Mater. Phys.* **1988**, *37*, 785−789.

(52) (a) Hariharan, P. C.; Pople, J. A. The influence of polarization functions on molecular orbital hydrogenation energies. *Theor. Chim. Acta* **1973**, *28*, 213−222. (b) Francl, M. M.; Pietro, W. J.; Hehre, W. J.; Binkley, J. S.; Gordon, M. S.; DeFrees, D. J.; Pople, J. A. Self-consistent molecular orbital methods. XXIII. A polarization-type basis set for second-row elements. *J. Chem. Phys.* **1982**, *77*, 3654−3665.

(53) Hay, P. J.; Wadt, W. R. Ab initio effective core potentials for molecular calculations. Potentials for the transition metal atoms Sc to Hg. *J. Chem. Phys.* **1985**, *82*, 270−283.

(54) Cossi, M.; Rega, N.; Scalmani, G.; Barone, V. Energies, structures, and electronic properties of molecules in solution with the C-PCM solvation model. *J. Comput. Chem.* **2003**, *24*, 669−681.

https://doi.org/10.1021/acs.inorgchem.2c03490
Inorg. Chem. XXXX, XXX, XXX−XXX